minerals

MDPI

Article

Chemical Composition and Petrogenetic Implications of Eudialyte-Group Mineral in the Peralkaline Lovozero Complex, Kola Peninsula, Russia

Lia Kogarko [1,*] and Troels F. D. Nielsen [2]

[1] Vernadsky Institute of Geochemistry and Analytical Chemistry, Russian Academy of Sciences, 119991 Moscow, Russia
[2] Geological Survey of Denmark and Greenland, 1350 Copenhagen, Denmark; tfn@geus.dk
* Correspondence: kogarko@geokhi.ru

Received: 23 September 2020; Accepted: 16 November 2020; Published: 20 November 2020

Abstract: Lovozero complex, the world's largest layered peralkaline intrusive complex hosts gigantic deposits of Zr-, Hf-, Nb-, LREE-, and HREE-rich Eudialyte Group of Mineral (EGM). The petrographic relations of EGM change with time and advancing crystallization up from Phase II (differentiated complex) to Phase III (eudialyte complex). EGM is anhedral interstitial in all of Phase II which indicates that EGM nucleated late relative to the main rock-forming and liquidus minerals of Phase II. Saturation in remaining bulk melt with components needed for nucleation of EGM was reached after the crystallization about 85 vol. % of the intrusion. Early euhedral and idiomorphic EGM of Phase III crystalized in a large convective volume of melt together with other liquidus minerals and was affected by layering processes and formation of EGM ore. Consequently, a prerequisite for the formation of the ore deposit is saturation of the alkaline bulk magma with EGM. It follows that the potential for EGM ores in Lovozero is restricted to the parts of the complex that hosts cumulus EGM. Phase II with only anhedral and interstitial EGM is not promising for this type of ore. Nor is the neighboring Khibiny complex despite a bulk content of 531 ppm of Zr. Khibiny only has interstitial and anhedral EGM. The evolution of the Lovozero magma is recorded in the compositions EGM up through a stratigraphy of 2400 m in Phase II and III of the complex, and distinct in elements like rare earth elements (REE), Sr, Ba, Th, U, Rb, Mn, Fe. The compositional evolution reflects primarily fractional crystallization processes within the magma chamber itself in combination with convective magma flow and layering by precipitation of minerals with different settling velocities. The suggested mechanism for the formation of the EGM deposits is flotation of very small, suspended EGM crystals in the convective magma and concentration below the roof of the magma chamber. Phase III EGM is enriched in total REE (1.3%) and in HREE (Ce/Yt = 8.8) and constitutes a world class deposit of REE in the million tons of Phase III eudialyte lujavrites.

Keywords: EGM; Lovozero; peralkaline nepheline syenites; EGM evolution

1. Introduction

High-field strength elements (HFSE) including the rare earth elements (REE) are strategic and critical for high-tech industry and green technologies. Their consumption and economic importance is progressively growing up. REE are for the most part mined in a restricted number of carbonatite-related deposits in which the REE are hosted in a large group of carbonate- and phosphor-bearing minerals including, bastnaesite, parisite, and monazite. A very different resource for HFSE (e.g., Zr, Hf, Nb, Ta, REE) is large-volume alkaline syenitic complexes rich in Eudialyte-Group Mineral (EGM) and other HFSE bearing minerals. The aim of this contribution is to improve our understanding of the formation

of HFSE resources in large alkaline complexes in order to define more effective exploration criteria for EGM-rich magmatic systems.

EGMs are complex zirconium silicates and typomorphic [1–4] for highly evolved agpaitic alkaline complexes. Agpaitic alkaline rocks have a bulk rock molar (Na + K)/Al > 1. Zircon is the typomorphic zirconium mineral in lesser alkaline miaskitic systems with an agpaitic index below 1.

More than 70 agpaitic intrusive complex are known world-wide, including the large Lovozero and Khibina complexes (Kola Peninsula, Russia), Ilimaussaq intrusion (Greenland), Pilanesberg (South Africa), or Poços de Caldas (Brazil). All show extreme enrichment in sodium (Na), volatiles (F, Cl, S), and have HFSE hosted in chemically complex minerals such as EGM, mosandrite-(Ce), keldyshite, lavenite, catapleiite, vlasovite, a. o. The very large tonnage of EGM-rich rocks in, e.g., the Lovozero complex suggests that it is one of the largest resources of Zr, REE, and other HFSE on earth and that it, as well as comparable large-volume alkaline complexes, may hold the HFSE resources for the future.

Studies of Rb-Sr, Sm-Nd, U-TH-Pb, Lu-Hf isotopic systems and of O, H [5–9] suggest that peralkaline magmatic systems are generally closed and inhibit the separation and loss of volatiles and the rare HFSE metals, i.e., REE, Zr, Hf, Nb, Ta, Th, U, Sr, Ba to late developed fluid phases [10]. The highly alkaline systems remain closed to these components leading to an extended interval of crystallization to very low temperatures [11–13]. This allows sub-liquidus mineral reactions, re-equilibration of parageneses, and a gradual transition from the magmatic to auto-metasomatic and hydrothermal stages. Residual melt and brines would concentrate ore components, e.g., in pegmatites. But such late accumulations would only form more local and smaller volume deposits, e.g., pegmatites and metasomatic zones. Large tonnage REE and HFSE deposits in alkaline complexes require large volumes of silicate melt to form and to be profitable scavenged at large scale. They would therefore likely form in the magma chamber during the crystallization of the bulk silicate melt.

The Eudialyte complex, hereafter Phase III, in the uppermost part of the Lovozero complex is rich in HFSE with layers composed of up to 95 vol. % EGM [1,14]. They are seemingly formed by classic accumulation of liquidus crystals of EGM and mat formation processes during the crystallization of bulk liquid in the magma chamber [15–17]. The EGMs of Lovozero show a wide variation in composition and therefore offer the possibility for the present study of compositional and morphological evolution of EGM and genesis of EGM ores.

2. Geology

The peralkaline Lovozero complex is one of the earth's largest layered agpaitic nepheline syenite-complexes. It is part of the Devonian Kola ultramafic–alkaline and carbonatitic province (KACP) which includes thousands of cubic kilometers of mafic to peralkaline and carbonatitic magma [5,18] (Figure 1). The Lovozero complex was emplaced centrally in Kola peninsula in Archaean basement and into a northwesterly striking tectonic zone that hosts a preserved E-W-trending belt of Paleozoic lithologies. The complex is rectangular in outline, has an area of 650 km^2, and exposes a 2400 m stratigraphic succession of undersaturated felsic plutonic rocks. The complex is depicted as trough-shaped with a feeding channel in the southwestern part of the intrusion [19]. The complex has attracted special interest because of enrichment in loparite-(Ce) and EGM, two rare minerals that are enriched in rare earths elements (REE), niobium, tantalum, zirconium, hafnium, and radioactive raw materials. Syenites, the largest of the KACP complexes, the Khibina alkaline complex, are exposed no more than 5 km west of Lovozero [20]. Khibiny is the host of major apatite-group mineral deposits.

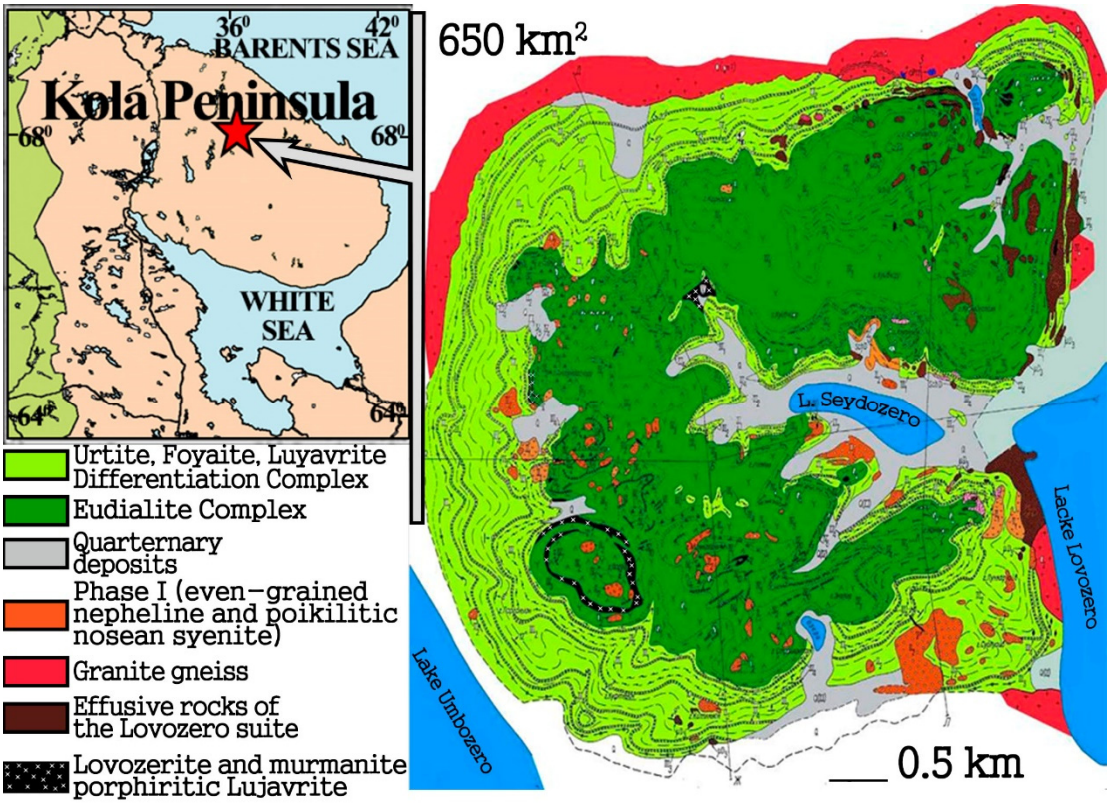

Figure 1. Geological map of the Lovozero intrusion with inset showing location of Lovozero (star) within the Kola Peninsula. Modified from Gerasimovsky et al. [1].

The alkaline rocks of Lovozero divide into three distinct phases. Phase I is preserved in the lowermost parts of the complex and as xenoliths throughout the complex. Phase I is composed of poikilitic, even-grained feldspathoidal syenite. Their bulk composition is miaskitic, i.e., have an agpaitic index (molar $(Na_2O + K_2O)/Al_2O_3$) > 1. The rock-forming minerals are K-Na feldspar, nepheline, nosean, aegirine-diopside, and magnesio-riebeckite with accessory ilmenite, magnetite, titanite, apatite group mineral and mosandrite (Ce).

Phase II, also known as the differentiated complex, is formed by repeated three-layer successions composed of urtite, followed by foyaite and lujavrite. Urtite is a syenite with a nepheline to pyroxene ratio > 0.7, foyaite is a nepheline-rich syenite, and lujavrite is a green peralkaline syenite rich in alkali pyroxene and feldspathoids. The transitions between the three rock types are mostly gradational. Sharp contacts only occur between the urtite and underlying lujavrite of the previous three-layers succession. The layered units of Phase II range in thickness from a few centimeters to hundreds of meter and sum to a total of app. 2000 m. The bulk compositions of Phase II nepheline syenites have an agpaitic index > 1 and are more alkaline than rocks of Phase I. The rock-forming minerals are nepheline, microcline, sodalite, aegirine, and arfvedsonite with accessory phases typomorphic for peralkaline syenites including EGM, lamprophyllite, lomonosovite, murmanite, apatite-group mineral, loparite-(Ce), villiaumite, titanite, sodalite, and lorenzenite (Table 1). Cumulus loparite-(Ce) locally appear concentrated into stratigraphically well constrained thin layers.

Table 1. Mineral formulae for the tipomorphic minerals of Lovozero.

Name	CNMMN/CNMNC Approved Formula
Barytolamprophyllite	$(BaK)Ti_2Na_3Ti(Si_2O_7)_2O_2(OH)_2$
Belovite-(Ce)	$NaCeSr_3(PO_4)_3F$
Cerite-(Ce)	$(Ce,La,Ca)_9(Mg,Fe^{3+})(SiO_4)_3(SiO_3OH)_4(OH)_3$
Lomonosovite	$Na_6Na_2Ti_2Na_2Ti_2(Si_2O_7)_2(PO_4)_2O_4$
Loparite-(Ce)	$(Na,Ce,Sr)(Ce,Th)(Ti,Nb)_2O_6$
Lorenzenite	$Na_2Ti_2O_3(Si_2O_6)$
Mosandrite-(Ce)	$(Ca_3REE)[(H_2O)_2Ca_{0.5}\square_{0.5}]Ti(Si_2O_7)_2(OH)_2(H_2O)_2$
Murmanite	$Na_2Ti_2Na_2Ti_2(Si_2O_7)_2O_4(H_2O)_4$
Nenadkevichite	$(Na, \square)_8Nb_4(Si_4O_{12})_2(O,OH)_4{\cdot}8H_2O$
Nordite-(Ce)	$Na_3SrCeZnSi_6O_{17}$
Steenstrupine-(Ce)	$Na_{14}Ce_6Mn^{2+}{}_2Fe^{3+}{}_2Zr(PO_4)_7Si_{12}O_{36}(OH)_2{\cdot}3H_2O$
Vitusite-(Ce)	$Na_3Ce(PO_4)_2$
Vuonnemite	$Na_6Na_2Nb_2Na_3Ti(Si_2O_7)_2(PO_4)_2O_2(OF)$

International Mineralogical Association (2020) [21].

The nepheline syenites of Phase III comprise 15–18% of the volume of the Lovozero complex and forms the upper sheet-like part of the Lovozero. The complex contains more than 120 pegmatites. The contact to the Phase II is conformable and sharp with dips shallowing toward the center of the complex. The eudialyte lujarites are exposed in the summits of the Lovozero Massif, have a maximum thickness of 450 m, of which an increasing part is lost to erosion toward the southeast. Phase III is composed of repeated units of urtite, juvite, eudialyte foyaite, and leucocratic, mesocratic, and melanocratic eudialyte lujavrites [1]. Juvite is a strongly nepheline- dominated rock with ~20 modal % alkali feldspar.

A coarse layering is developed in the eudialyte lujavrites. Their bulk rock compositions are very alkaline with an agpaitic index of ~1.50 and they are rich in high field strength elements (HFSE) such as zirconium that reaches a bulk rock maximum of 1.66 wt. % ZrO_2 [8]. Bodies of porphyritic lujavrite are located at the contact to the underlying Phase II syenites. They are believed to be partly quenched melts or mushes of eudialyte lujavrite magma. The eudialyte lujavrites host a suite of later intrusive lithologies including veins of lovozerite and murmanite and lamprophyllite porphyritic lujavrite, (about 2 vol. % of Phase III). They are interpreted as residual melts of Phase III are up to several kilometers in length and up to 50 m wide. Other late intrusive bodies are composed of poikilitic sodalite syenite and tawite (sodalite dominated rock). Titanite, apatite-group mineral, and amphibole-rich rocks in the eastern part of the complex are formed in a reaction between the Phase III magma and host rocks in the roof of the Lovozero complex [1].

The main rock-forming minerals of eudialyte-lujavrites are nepheline (23%), aegirine (17%), alkali-amphibole (15%), microcline (20%), and EGM (about 25%). EGM occurs as euhedral crystals and grain cores, a distinctive characteristic that sets EGM of Phase III apart from the EGMs of Phase II. The common accessory minerals include lamprophyllite, lomonosovite, murmanite, loparite-(Ce), lovozerite, pyrochlore supergroup minerals, and sodalite. The modal proportion of EGM crystals increases significantly to 30–40 vol. % in upper parts of Phase III. These EGM-rich rocks of ore grade are found in the apical part of the eudialyte complex as layers and meter-size lenticular bodies. Horizons defined as eudialyte ore are almost monomineralic with up 95 vol. % EGM with minor nepheline, aegirine, microcline, and arfvedsonite. EGM ores are a significant resource for especially the heavy rare earths elements (HREE), zirconium, and hafnium. In addition, the ores are also enriched in manganese, niobium, scandium, uranium, and thorium.

3. Samples and Analytical Method

Most of the samples in this study were collected from seven drill cores (numbers 469, 904, 521, 178, 144, 272B and 905) that cover a complete stratigraphic section through the Lovozero complex (~2400 m) except for the middle part of Phase II. Hand samples completed the vertical section of Lovozero.

The EGM analyses were made using Cameca SX50 and CAMECASX 100 electron microprobes with four wavelength-dispersive spectrometers at the Natural History Museum, London, and at Vernadsky Institute, Moscow. Operating conditions were in both cases an accelerating voltage of 15 kV and a 20 nA probe current. A combination of natural minerals, synthetic compounds, and pure metals, which included synthetic $NaNbO_3$, $SrTiO_3$, $CaTiO_3$, $ZrSiO_4$ and individual REE-doped glasses for the major components were used as standards.

Trace element analyses were performed in Frankfurt University, Max Plank Institute in Mainz, Germany, and Vernadsky Institute, using Thermo Scientific Element 2 ICPMS instruments coupled with a Resonetics Resolution M-50 excimer laser. The laser spot size varied from 20 to 60 µm. NIST glasses and Zircon 91500 were used as standards. To minimize the influence of later rimming and equilibrations of first crystallized EGM, only the cores of EGM grains and crystals were analyzed. The full data set includes analyses from 650 grains in 213 samples.

4. Results

4.1. Petrographic Characteriatics of EGM

Detailed accounts of the petrography of the lithologies of the Lovozero complex can be found in Vlasov et al. [14], Gerasimovsky et al. [1], and Bussen and Sakharov [22]. The rock-forming paragenesis remains the same throughout Lovozero, and includes nepheline, potassium feldspar, aegirine, and alkali-amphibole. Only the relative proportion and the compositions of the rock-forming minerals vary. The present work focusses on the petrographic relations and compositions of EGM.

Eudialyte is not present in Phase I lithologies, which therefore will not be described further. In the lower miaskitic part of Phase II the accessory phases include zircon, manganese-rich ilmenite, mosandrite-(Ce), keldyshite, lavenite, titanite, apatite group minerals, and no EGM. Zircon is the mineral that hosts the Zr. EGM is found higher in Phase II in association with agpaitic minerals such as lorenzenite, lamprophyllite, villiaumite, murmanite, and lomonosovite. In these rocks, EGM occurs as interstitial and anhedral grains. The size of EGM grains varies from tens to 1–2 mm. Individual EGM grains display very complex zoning that shows well in back-scattered electron images (Figure 2).

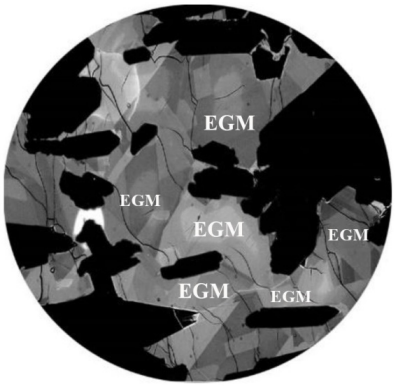

Figure 2. Backscatter image of xenomorphic and interstitial Eudialyte Group of Mineral (EGM) (grey) in foyaite of the Phase II. All other phases including pyroxene, alkali feldspar, and nepheline are black. Field of view 1.5 mm.

EGM occurs as euhedral crystals throughout the overlying Phase III eudialyte lujavrites. The crystals are 2–4 mm in size, increasing to 5 mm in eudialyte "ore" (Figures 3 and 4). The EGM

crystals of Phase III show sector and oscillatory zoning [1]. In the upper part of Phase III the EGM grains of a given sample have a very uniform size and some contain fragments of small, broken crystals (Figure 5). They are especially common in the part of eudialyte ores in the uppermost part of the complex.

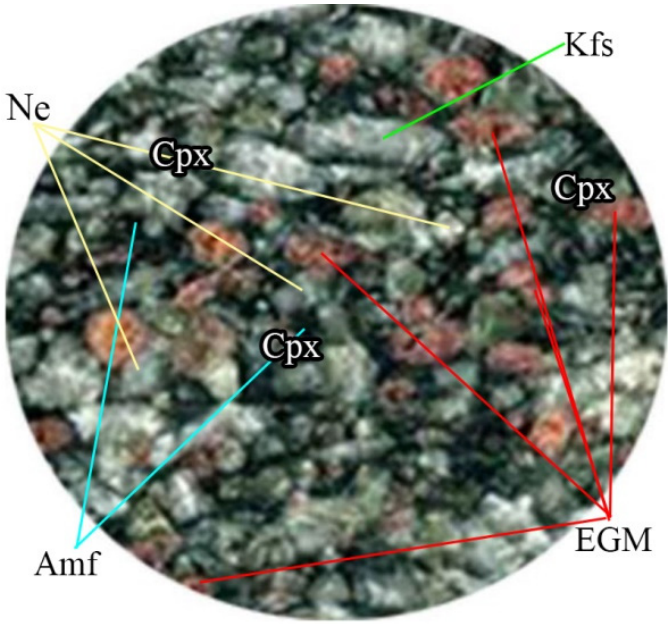

Figure 3. Eudialyte lujavrite, with idiomorphic crystals of EGM. Transmitted light, field of view 30 mm.

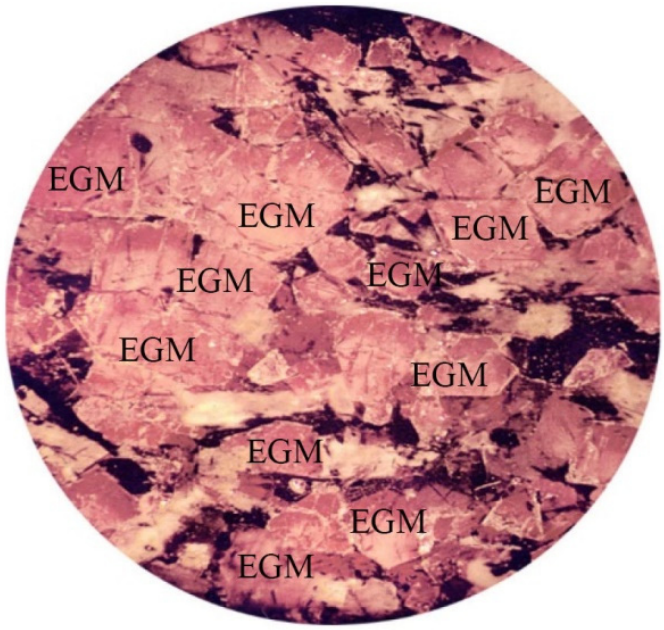

Figure 4. EGM ore composed of idiomorphic crystal, from the uppermost part of the Phase III. Transmitted light, field of view 25 mm.

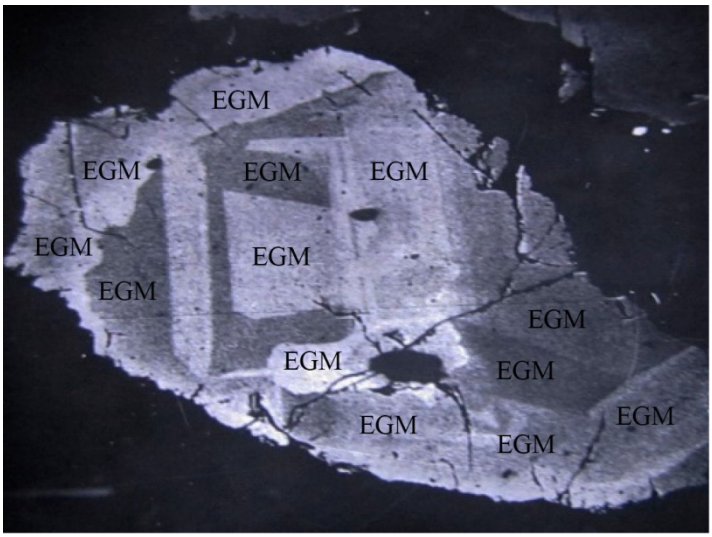

Figure 5. Backscatter electron image of an EGM crystal from ore containing composed of fragments of EGM crystals (Field of view 1 mm).

4.2. Compositions of EGM

EGM is a complex mineralogical group with many compositional endmembers [23]. Lovozero EGM is dominated by "common" eudialyte, with proportions of raslakite ($Na_{15}Ca_3Fe^{2+}{}_3(Na,Zr)_3Zr_3(Si,Nb)(Si_{25}O_{73})(OH,H_2O)_3(Cl,OH)$), taseqite ($Na_{12}Sr_3Ca_6Fe_3Zr_3Nb(Si_{25}O_{73})Cl_2(O,OH,H_2O)_{3)}$, and sergevanite $Na_{15}(Ca_3Mn_3)(Na_2Fe)Zr_3(Si_{26}O_{72})(OH)_3{\cdot}H_2O$) [24].

Calculated average concentrations of Sr, Ba, Rb, REE (La, Ce, Yb), Th, U, Mn, Fe in EGMs of Phase II and Phase III rocks are shown in Table 2, Table 3, Table 4 and Table 6, and chondrite normalized REE spectra, ∑LREE versus ∑HREE concentrations, and spidergrams normalized to primitive mantle are shown in Figures 6–8.

Table 2. Representative electron microprobe (EMP) compositions of EGM from Phase II.

Sample	382	383	385	389	390	392	393	399	401	402
Nb_2O_5	1.09	1.14	0.72	1.77	0.79	1.06	0.67	0.48	0.48	0.88
TiO_2	0.33	0.37	0.62	1.33	0.41	0.38	0.41	0.48	0.48	0.48
ZrO_2	12.33	12.81	15.90	9.90	13.62	12.81	14.41	14.55	13.65	13.59
HfO_2	0.20	0.23	0.35	0.14	0.28	0.32	0.34	0.20	0.25	0.28
ThO_2	0.00	0.00	0.00	0.00	0.00	0.00	0.00	0.10	0.10	0.10
UO_2	0.00	0.00	0.00	0.00	0.00	0.00	0.00	0.16	0.10	0.10
SiO_2	49.40	49.99	48.44	49.62	48.27	48.83	48.72	49.35	48.98	48.54
Al_2O_3	0.00	0.00	0.00	0.00	0.00	0.00	0.00	0.20	0.22	0.16
Y_2O_3	0.21	0.25	0.52	0.22	0.56	0.63	0.57	0.69	0.68	0.35
La_2O_3	0.58	0.50	0.29	0.50	0.39	0.44	0.37	0.19	0.24	0.37
Ce_2O_3	1.26	1.24	0.63	1.23	0.81	0.93	0.78	0.66	0.63	0.74
Pr_2O_3	0.28	0.17	0.15	0.15	0.15	0.15	0.15	0.15	0.15	0.15
Nd_2O_3	0.54	0.52	0.29	0.47	0.40	0.48	0.47	0.39	0.26	0.35
CaO	7.96	8.14	4.76	8.81	7.50	7.48	6.70	6.38	7.07	7.14
MgO	0.00	0.00	0.00	0.00	0.00	0.00	0.00	0.05	0.05	0.05
MnO	3.09	2.92	2.42	3.03	1.82	2.27	1.70	2.93	2.76	3.27
FeO	1.68	1.57	3.09	0.80	4.34	4.02	4.75	1.22	0.95	1.10
SrO	1.86	1.66	0.98	3.02	0.92	1.12	0.77	1.36	1.56	1.93
BaO	0.52	0.35	0.07	0.69	0.04	0.14	0.05	0.29	0.28	0.24
Na_2O	16.71	16.70	16.97	14.39	15.96	16.05	15.84	15.70	14.59	15.67
SO_3	0.54	0.37	0.27	0.43	0.15	0.16	0.22	0.18	0.20	0.24
Cl	0.54	0.50	1.12	0.50	1.25	1.36	1.24	1.14	1.15	0.76
Total	99.12	99.43	97.59	97.00	97.66	98.63	98.16	96.85	94.83	96.49
O=Cl	0.12	0.11	0.25	0.11	0.28	0.31	0.28	0.26	0.26	0.17

Table 2. *Cont.*

Sample	382	383	385	389	390	392	393	399	401	402
TOTAL	99.00	99.32	97.34	96.89	97.38	98.32	97.88	96.59	94.57	96.32
					A.P.F.U.					
Nb	0.26	0.27	0.17	0.41	0.19	0.25	0.16	0.11	0.11	0.21
Ti	0.13	0.14	0.25	0.52	0.16	0.15	0.16	0.19	0.19	0.19
Zr	3.13	3.22	4.13	2.49	3.55	3.29	3.73	3.72	3.52	3.52
Hf	0.03	0.03	0.05	0.02	0.04	0.05	0.05	0.03	0.04	0.04
Th	0.00	0.00	0.00	0.00	0.00	0.00	0.00	0.01	0.01	0.01
U	0.00	0.00	0.00	0.00	0.00	0.00	0.00	0.02	0.01	0.01
Si	25.74	25.73	25.83	25.59	25.81	25.75	25.84	25.89	25.89	25.79
Al	0.00	0.00	0.00	0.00	0.00	0.00	0.00	0.12	0.14	0.10
Y	0.06	0.07	0.15	0.06	0.16	0.18	0.16	0.19	0.19	0.10
La	0.11	0.09	0.06	0.10	0.08	0.09	0.07	0.04	0.05	0.07
Ce	0.24	0.23	0.12	0.23	0.16	0.18	0.15	0.13	0.12	0.14
Pr	0.05	0.03	0.03	0.03	0.03	0.03	0.03	0.03	0.03	0.03
Nd	0.10	0.10	0.06	0.09	0.08	0.09	0.09	0.07	0.05	0.07
Ca	4.44	4.49	2.72	4.87	4.30	4.23	3.81	3.59	4.00	4.06
Mg	0.00	0.00	0.00	0.00	0.00	0.00	0.00	0.04	0.04	0.04
Mn	1.36	1.27	1.09	1.32	0.82	1.01	0.76	1.30	1.24	1.47
Fe	0.73	0.68	1.38	0.35	1.94	1.77	2.11	0.54	0.42	0.49
Sr	0.56	0.50	0.30	0.90	0.29	0.34	0.24	0.41	0.48	0.59
Ba	0.11	0.07	0.01	0.14	0.01	0.03	0.01	0.06	0.06	0.05
Na	16.88	16.67	17.54	14.39	16.55	16.41	16.29	15.97	14.95	16.14
S	0.21	0.14	0.11	0.17	0.06	0.06	0.09	0.07	0.08	0.10
Cl	0.48	0.44	1.01	0.44	1.13	1.22	1.11	1.01	1.03	0.68

The basis for APFU calculations Si + Nb = 26.

Table 3. Representative ICPMS trace element analyses of EGM from Phase II.

Element (ppm)	01-1	01-2	01-3	02-1	02-2	02-3	1610-03	1610-04	463-04	1610-06
Sc	102	104	108	117	120	120	119	121	79	111
Ti	1331	1374	1257	1267	1333	1276	1340	1419	1207	1318
Mn	8518	8704	8581	7632	8662	8144	8306	8657	7609	7894
Co	0.16	0.17	0.15	0.2	0.23	0.18	0.18	0.2	–	0.2
Cu	0.85	1.08	1.06	1.21	1.14	1.08	1.27	1.13	0.75	1.24
Rb	6.74	7.61	7.51	7.82	8.55	7.91	8.52	8.93	2.85	7.52
Sr	2880	2872	2841	2773	2815	2738	2837	2937	3273	2632
Y	1487	1471	1483	1453	1477	1404	1307	1414	1045	1324
Nb	2600	2469	2168	2112	2177	2119	2128	1988	1327	2090
Ba	22	20	21	15	16	15	25	17	459	15
La	1703	1627	1536	1462	1512	1450	1438	1429	1178	1435
Ce	3049	2943	2787	2634	2782	2705	2543	2612	2324	2602
Pr	349	337	315	304	315	322	303	306	273	304
Nd	1455	1437	1311	1312	1315	1322	1292	1321	1145	1256
Sm	364	347	336	322	331	328	316	336	283	308
Eu	104	103	95	92	96	98	94	95	78	88
Gd	309	302	274	267	297	288	270	268	249	259
Tb	52	50	50	46	47	45	45	43	37	43
Dy	270	262	269	253	256	244	241	243	204	238
Ho	55	50	52	48	52	50	45	47	39	46
Er	145	130	134	124	130	132	116	121	95	116
Tm	20	19	19	18	19	19	17	18	13	16
Yb	131	120	118	116	117	112	109	116	83	108
Lu	15	15	14	14	14	14	13	14	11	13
∑REE	8021	7742	7310	7012	7283	7128	6842	6969	6010	6832
Ce/Yb	23	25	24	23	24	24	23	22	28	24
Hf	1075	1067	1039	1058	1046	1069	1112	1123	789	1126
Ta	287	270	181	184	187	193	217	222	127	188
Pb	31	31	26	23	26	24	31	27	5	25
Th	20	21	18	19	20	19	19	17	28	18
U	25	24	22	23	22	21	22	22	39	22

Table 4. Representative EMP compositions of EGM from Phase III.

Sample	778	153	290	1	373	304	779	336	335
Nb_2O_5	0.76	0.67	0.75	0.99	0.51	0.77	0.71	0.73	0.61
TiO_2	0.63	0.53	0.6	0.58	0.65	0.48	0.52	0.49	0.67
ZrO_2	14.28	13.42	13.53	13.26	13.81	13.03	13.35	13.37	14.22
HfO_2	0.00	0.27	0.29	0.41	0.00	0.27	0.26	0.22	0.00
SiO_2	49.49	50.09	49.95	48.84	50.19	49.39	49.81	50.27	50.04
Al_2O_3	0.20	0.00	0.00	0.16	0.23	0.14	0.15	0.11	0.16
Y_2O_3	0.69	0.7	0.63	0.7	0.56	0.57	0.85	0.33	0.34
La_2O_3	0.36	0.19	0.34	0.19	0.28	0.18	0.33	0.15	0.27
Ce_2O_3	0.71	0.63	0.57	0.6	0.51	0.58	0.66	0.38	0.66
Pr_2O_3	0.00	0.15	0.15	0.15	0.00	0.00	0.00	0.00	0.00
Nd_2O_3	0.43	0.31	0.37	0.37	0.4	0.32	0.35	0.41	0.34
Sm_2O_3	0.23	0.00	0.00	0.00	0.00	0.00	0.12	0.17	0.00
Gd_2O_3	0.11	0.00	0.00	0.00	0.26	0.00	0.00	0.26	0.32
CaO	8.28	7.24	7.3	8.02	7.97	7.68	8.45	8.65	7.93
MgO	0.04	0.00	0.00	0.07	0.10	0.04	0.01	0.05	0.05
MnO	1.86	2.3	1.99	2.13	1.97	3.20	1.91	2.05	2.02
FeO	3.42	3.15	3.89	3.13	4.92	4.34	3.24	5.27	4.76
SrO	0.83	1.49	1.35	2.19	0.51	0.63	0.85	0.52	0.69
BaO	0.11	0.10	0.11	0.01	0.11	0.00	0.10	0.18	0.09
Na_2O	16.24	16.98	16.18	16.24	15.41	15.82	16.14	15.22	14.92
K_2O	0.28	0.3	0.38	0.25	0.29	0.21	0.28	0.22	0.29
SO_3	0.26	0.18	0.26	0.18	0.28	0.18	0.20	0.25	0.30
Cl	1.43	1.40	1.40	1.58	1.31	1.32	1.44	1.42	1.39
TOTAL	100.64	100.1	100.04	100.05	100.27	99.15	99.73	100.72	100.07
O=Cl	0.32	0.32	0.32	0.36	0.30	0.30	0.32	0.32	0.31
TOTAL	100.32	99.78	99.72	99.69	99.97	98.85	99.41	100.40	99.76
				A.P.F.U.					
Nb	0.18	0.16	0.18	0.24	0.12	0.18	0.17	0.17	0.14
Ti	0.25	0.21	0.23	0.23	0.25	0.19	0.20	0.19	0.26
Zr	3.63	3.38	3.41	3.41	3.47	3.32	3.38	3.35	3.58
Hf	0.00	0.04	0.04	0.06	0.00	0.04	0.04	0.03	0.00
Si	25.82	25.84	25.82	25.76	25.88	25.82	25.83	25.83	25.86
Al	0.12	0.00	0.00	0.10	0.14	0.09	0.09	0.07	0.10
Y	0.19	0.19	0.17	0.20	0.15	0.16	0.23	0.09	0.09
La	0.07	0.04	0.06	0.04	0.05	0.03	0.06	0.03	0.05
Ce	0.14	0.12	0.11	0.12	0.10	0.11	0.13	0.07	0.12
Pr	0.00	0.03	0.03	0.03	0.00	0.00	0.00	0.00	0.00
Nd	0.08	0.06	0.07	0.07	0.07	0.06	0.07	0.07	0.06
Sm	0.04	0.00	0.00	0.00	0.00	0.00	0.02	0.03	0.00
Gd	0.02	0.00	0.00	0.00	0.04	0.00	0.00	0.04	0.05
Ca	4.63	4.00	4.04	4.53	4.40	4.30	4.70	4.76	4.39
Mg	0.03	0.00	0.00	0.06	0.08	0.03	0.01	0.04	0.04
Mn	0.82	1.01	0.87	0.95	0.86	1.42	0.84	0.89	0.88
Fe	1.49	1.22	1.51	1.24	1.91	1.71	1.41	2.26	1.85
Sr	0.25	0.45	0.40	0.67	0.15	0.19	0.25	0.15	0.21
Ba	0.02	0.02	0.02	0.00	0.02	0.00	0.02	0.04	0.02
Na	16.43	16.99	16.22	16.61	15.41	16.04	16.23	15.17	14.95
K	0.19	0.20	0.25	0.17	0.19	0.14	0.19	0.14	0.19
S	0.10	0.07	0.10	0.07	0.11	0.07	0.08	0.10	0.12
Cl	1.26	1.22	1.23	1.41	1.15	1.17	1.27	1.23	1.22

The basis for APFU calculations Si + Nb = 26.

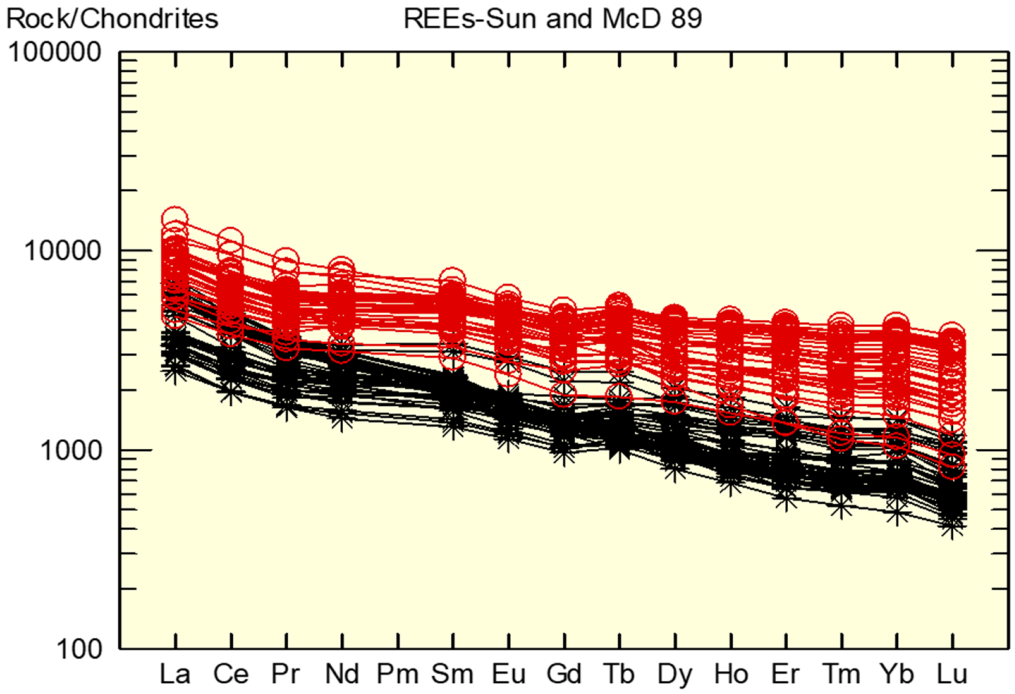

Figure 6. Distribution of rare earth elements (REE) in Lovozero EGM of Phase II (black) and of Phase III (red).

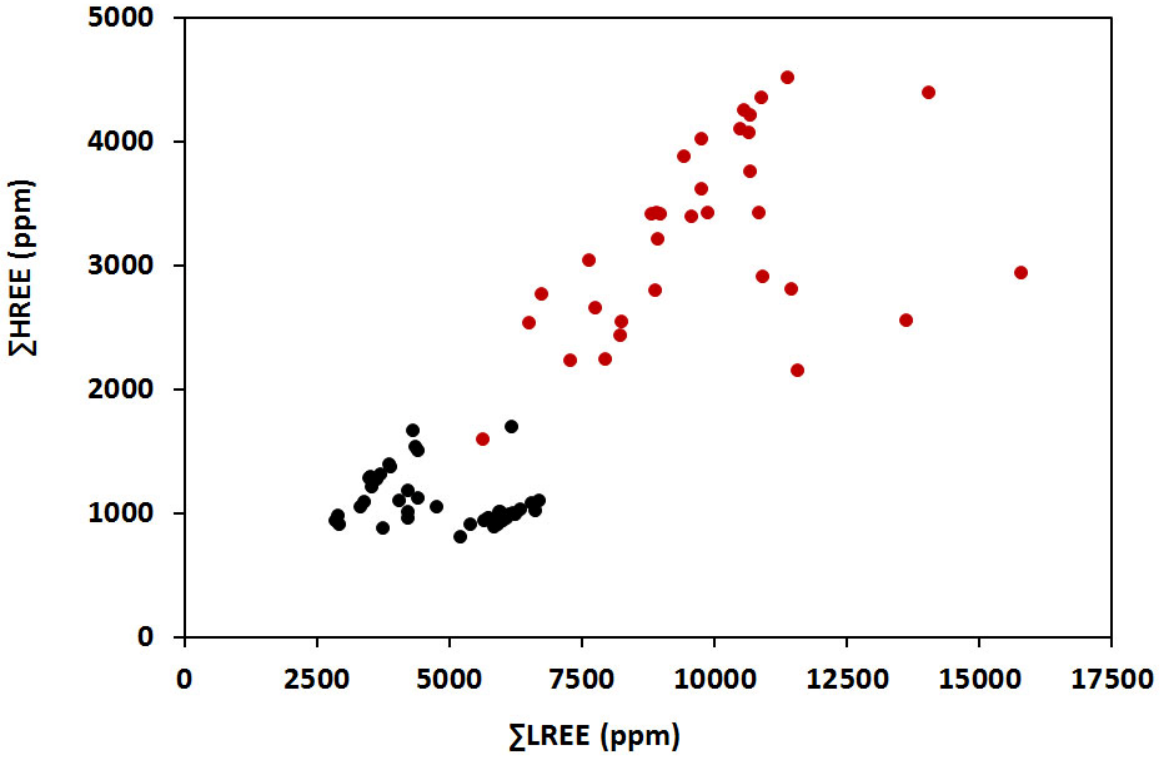

Figure 7. ∑LREE versus ∑HREE in EGM. Black dots: Phase II; red dots: Phase III.

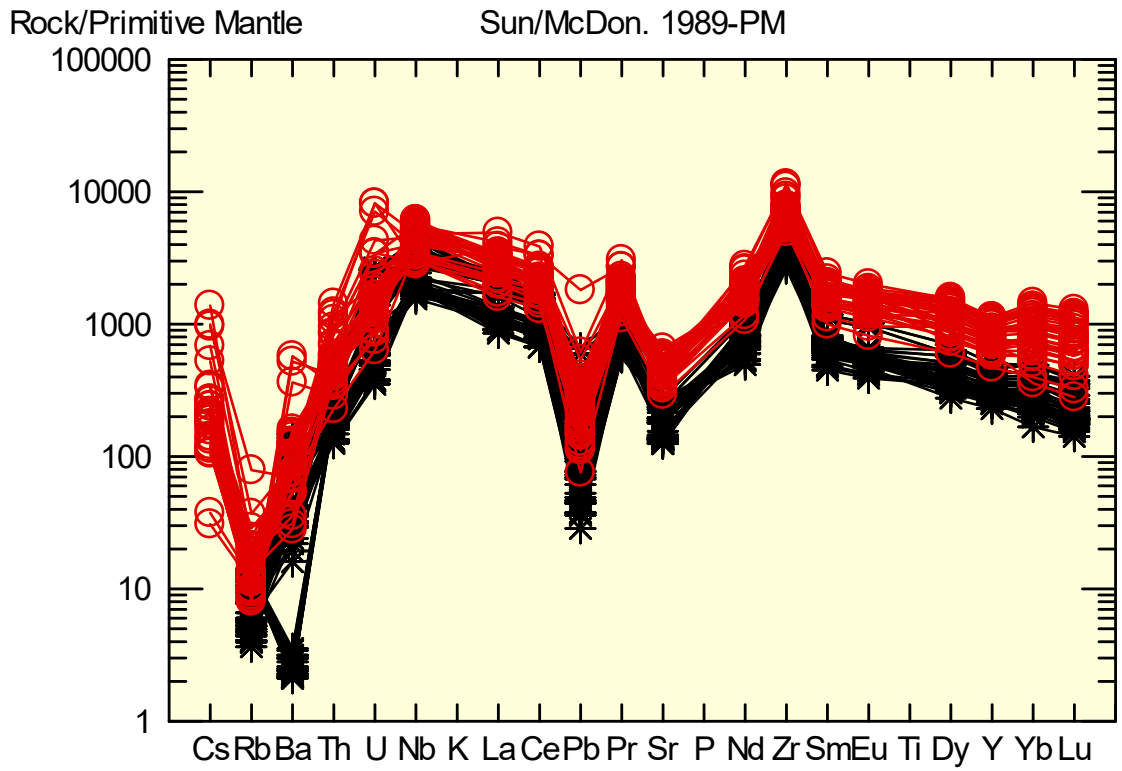

Figure 8. Spidergram for EGM of differentiated (black) and eudialyte (red) complexes of Lovozero.

The EGM of the Phase II is REE enriched and reaches ~0.8 wt. % and has from c. 600 to 1700 ppm La and from c. 100 to 180 ppm Yb corresponding to chondrite normalized ratios of ~2500 to ~7000 c. and ~300 to ~1100, respectively (Figure 6). In ∑LREE versus ∑HREE (Figure 7) the analyses of Phase II EGM are divided into two well-defined groups with a small number of compositions in between. EGMs of individual samples of Phase II appear to have very similar ratios, though with variations in ∑REE. Compared to the Phase II the EGMs of the Phase III have elevated ∑REE contents reaching 1.8 wt. %. and have from c. 1100 to 3400 ppm La and from 200 to ~3000 ppm Yb corresponding to chondrite-normalized ratios of ~5000 to ~15000 and ~800 to ~1100, respectively (Figure 6). In ∑LREE versus ∑HREE (Figure 7) Phase III EGMs, except for a small number of outliers, form a suite with a steep trend similar to that of the HREE-rich Phase II EGMs. Average EGM of Phase III has Ce/Yb = 8.88 and 15.23 in EGM of the Phase II (Table 6).

The EGM composition shows continuous upwards decrease in Fe and a complementary increase in Mn from Phase II to the Phase III. The Mn/Fe ratios (apfu) increase upward from 0.76 in the Phase II to 0.87 in EGM of Phase III (Figure 9, Tables 2 and 4, average values in Tables 5 and 6). Shilling et al. [25] considered Mn/Fe ratio to be the most suitable fractionation indicator. The difference in Mn/Fe ratio in EGMs of Phase II and Phase III is insignificant. Consequently, the values of the Mn and Fe distribution coefficients of surrounding minerals mainly affected this ratio. Trace element compositions normalized to primitive mantle (Figure 8) show very similar patterns for all EGM though with overall higher concentrations in the EGMs of Phase III. Nb, Ti, and Hf increase from 1872, 1237, 963 to 3242, 1455, 2076, respectively. U and Th are enriched in EGM of the eudialyte complex. The spidergrams show expected peaks at Zr and Nb, and low peaks at Sr, Pb, Ba and Rb. In contrast to most other elements Pb, U, Th, Ba, Rb, Cs show up to 10 variation in normalized values.

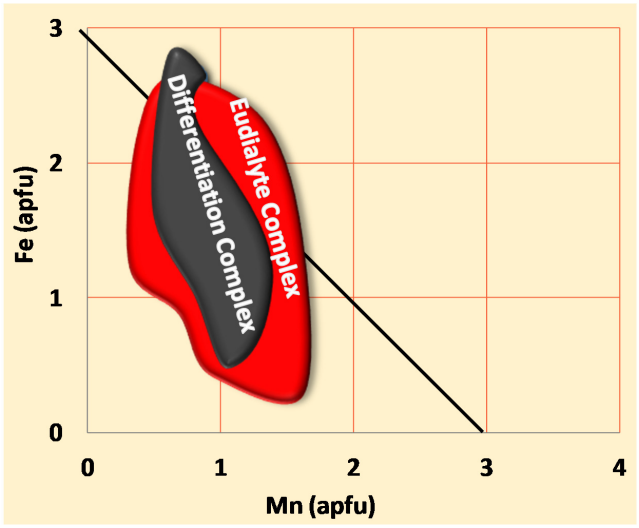

Figure 9. Variation of Fe and Mn in differentiated (black) and eudialyte (red) complexes.

Table 5. Representative ICPMS trace element analyses of EGM from the Phase III.

Element (ppm)	1a	1b	5b	9a	8b	2a	3a	3b	3c	4a
Sc	75.21	63.06	69.18	63.08	53.95	52.56	47.5	48.11	53.65	47.76
Ti	1302	1313	1257	1081	1459	1158	1104	1106	1237	1177
Mn	11,507	11,832	12,315	13,011	18,159	19,263	15,488	15,575	16,525	20,349
Co	81.8	17.6	94.86	102.75	–	–	–	–	–	–
Cu	16.22	3.19	19.35	21.19	–	–	–	–	–	–
Rb	8.68	15.33	8.78	5.66	7.81	7.46	5.39	6.44	7.22	7.1
Sr	7004	7632	6185	7118	10,434	12,501	11,673	11,971	12,443	9446
Y	2924	3384	2143	3288	4851	3999	3916	3927	4191	2867
Nb	2202	2206	2177	2585	3511	3715	3703	3874	4051	3199
Ba	197	216	523	488	677	392	639	534	600	980
La	1188	1505	1107	1373	2144	1751	2079	1820	2031	1687
Ce	2548	3205	2320	2703	4383	3538	3939	3607	3946	3389
Pr	367	422	306	340	564	472	497	470	508	436
Nd	1973	1991	1460	1591	2705	2366	2313	2320	2460	2071
Sm	653	617	443	502	872	778	744	764	815	639
Eu	217	199	138	161	291	269	257	269	278	215
Gd	718	607	387	513	913	802	769	799	833	616
Tb	137	115	69	100	184	153	150	154	163	112
Dy	666	731	442	703	1 099	905	895	895	959	635
Ho	144	147	86	149	236	187	187	187	199	129
Er	395	395	226	413	665	506	517	507	542	339
Tm	57	56	31	59	97	72	74	72	76	47
Yb	382	365	196	388	648	472	487	467	501	308
Lu	49	46	24	49	86	60	62	60	64	39
∑REE	9494	10,399	7235	9045	14,885	12,331	12,971	12,391	13,376	10,661
Ce/Yb	6.66	8.77	11.83	6.97	6.76	7.5	8.08	7.73	7.88	11.02
Hf	1809	1557	1229	1291	2421	1854	1809	1870	2072	1785
Ta	198	182	145	194	303	371	387	429	423	351
Pb	9.2	12.98	10.33	5.39	11.53	14.65	8.65	10.9	10.24	18.96
Th	34.13	31.65	29.11	19.47	41.06	36.88	41.57	37.61	45.42	40.66
U	31.5	28.28	30.63	13.37	30.97	22.7	18.96	23.36	26.64	26.33
Li	5.84	5.31	4.6	7.54	–	3.03	–	–	–	–
Be	0.78	1.21	3.48	1.27	2.69	8.97	11.43	4.43	8.35	4.94
B	87.43	–	–	–	25.41	38.49	34.1	40.7	37.46	46.89
V	1.85	1.55	2.1	1.73	2.8	1.71	1.85	2.04	2.09	2.43
Ni	4.3	–	4.69	5.78	–	–	–	2.35	–	–
Zn	11.38	22.88	18.9	18.2	23.41	54.74	22.35	21.72	24.51	58.37
Ga	41.24	15.38	52.86	44.48	12.86	12.68	18.04	14.63	16.55	12.22
Cs	1.49	1.67	1.63	1.12	1.52	1.49	0.92	1.06	1.58	4.14

Table 6. Average compositions of EGM in Phase II and Phase III.

Element	Phase II ppm	Phase III ppm	Element	Phase II ppm	Phase III ppm
Sc	85.96	57.26	Er	156	483
Ti	1237	1455	Tm	22	68.95
Co	4.18	74.25	Yb	143	454
Cu	1.59	14.99	Lu	17.11	58.64
Rb	5.5	10.61	∑REE	6038	13,013
Sr	3762	9828	Ce/Yb	15.23	8.88
Y	1505	3811	Hf	963	2076
Nb	1872	3242	Ta	179	293
Ba	249	891	Pb	17.71	20.99
La	1166	1980	Th	19.4	50.91
Ce	2181	4032	U	23.64	47.63
Pr	265	517	Li	–	5.45
Nd	1161	2475	Be	–	5.61
Sm	317	762	B	–	34.93
Eu	97.51	249	V	–	2.63
Gd	292	760	Ni	–	3.96
Tb	51.04	145	Zn	–	69.38
Dy	299	851	Ga	–	21.97
Ho	58.61	177	Cs	–	2.33

5. Discussion

5.1. Arrival of EGM on Liquidus

The timing of crystallization of EGM relative to that of the liquidus paragenesis of its host, and the compositional variations of the EGMs provide constrains to the genesis of large deposits of EGM with high concentrations of valuable HREE. In Phase II of Lovozero, EGM is an interstitial and poikilitic phase. It has anhedral grain shapes and shows significant and non-systematic chemical zonation (Figure 2). This type of EGM is typical for all parts of Phase II, with modal proportion of EGM, lamprophyllite, murmanite, and lomonosovite increasing upwards toward Phase III. The petrographic relations suggest that the anhedral EGM grains crystallized from late stage melts in Phase II crystal mushes, and that local geochemical variation, coexisting with HFSE-bearing accessory phases, and diffusion of HFSE account for the compositional variability in, e.g., ∑LREE/∑HREE (Figure 7).

The petrographic relations are very different for EGM in Phase III and the eudialyte deposits. EGM grains are euhedral (Figures 3 and 4), and some are composed of amalgamated fragments of EGM crystals (Figure 5). The EGM crystals are understood as liquidus crystals that crystallized in equilibrium with the lujavritic liquidus paragenesis, that includes nepheline, aegirine, and alkali-amphibole. Support for EGM as liquidus phase in melt of Phase III and eudialyte ores is provided by the porphyritic lujavrites. In these partly quenched rocks very small euhedral EGM crystals are enclosed other liquidus phases (Figure 10).

Although the ∑LREE/∑HREE ratios and concentrations vary and outliers occur, the ratios of Phase III EGMs are in the 2–3 range and suggest a general equilibration with a single and large volume of melt. That is a characteristic of liquidus phases, and the main control on the formation of EGM ores in Lovozero is therefore, suggested to be saturation of agpaitic magma in components necessary for nucleation of, liquidus eudialyte i.e., in the melt with 1–2% ZrO_2. Such concentrations are found in quenched and homogenized melt inclusions in the minerals of EGM ores and experiments [13].

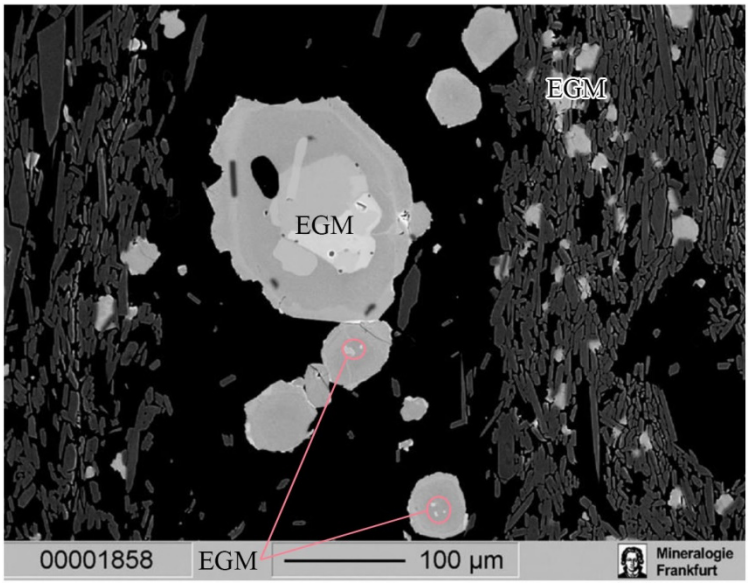

Figure 10. Backscattered electron image of a porphyritic EGM (white) lujavrite (polished thin section).

5.2. Genesis of the Lovozero EGM Ore

The timing of arrival of EGM on the liquidus in the Lovozero complex is here estimated from the relative volumes of the phases of the complex, and assuming a continuum of fractionation and melt evolution. Phase III comprises the last 15 vol. % that crystallized in Lovozero, and the bulk magma apparently saturated with EGM after ~85% of the initial volume of Lovozero had solidified. Following Gerasimovsky et al. [1] the initial ZrO_2 content of the bulk liquid Lovozero complex was 0.35 wt. %. With crystallization and evolution of Lovozero, the ZrO_2 content is modelled to have reached 1.66 wt. %. in Phase III [7]. This corroborates the experimentally estimated concentration of 1.4–2 wt. % ZrO_2 needed to bring EGM on the liquidus of alkaline agpaitic magma [13], and thus a classic fractional crystallization scenario.

Crystals of EGM form mats in the uppermost parts of in Phase III. The density of eudialyte is in the order of 2.8. The agpaitic magma of Ilimaussaq intrusion is and a proxy for that of Lovozero has a modelled density of ~2.3. It does not seem reasonable to assume the EGM mats to be simple floatation cumulates. The small euhedral crystals with sizes in the hundredths of a millimeter, in particular in the porphyritic lujavrites, would be in suspension and be carried along in convective magma. The here preferred genesis is therefore floatation of tiny crystals of EGM to the top of Phase III melt volume, where they are envisaged to have stuck together and re-crystallize to larger crystals in a type of ripening process (Figure 4). A similar mechanism for the accumulation and concentration of heavier apatite-group mineral and lighter nepheline was envisaged in the model proposed for the Genesis of Apatite ores in the Khibiny complex [26].

The EGMs of Phase III lujavrites and eudialyte ores have elevated HREE contents compared to EGMs of Phase II. The anhedral Phase II EGMs are confined to interstitial volumes of melt which evolved relative to the contemporaneous bulk liquid. Interstitial EGM would start to crystallize in mushes of Phase II, before the arrival of EGM on the liquidus of the bulk liquid of Phase III. The EGMs of Phase II would be trapped in small volumes of melt and not be able to scavenge HFSE elements from a larger bulk magma. They would have compositions controlled by the bulk composition of the interstitial melts, and as suggested in Figure 7, the paragenesis of coexisting HFSE-bearing phases.

On the contrary we suggest that the euhedral and idiomorphic liquidus crystals of EGM of Phase III crystalized in a large convective volume of melt in equilibrium with the rock-forming liquidus paragenesis and layering in Phase III lujavrites. They also formed after crystallization of loparite-(Ce)

and formation of the loparite ores. Loparite-(Ce) is very strongly enriched in LREE and the effect would be a relative enrichment in HREE over LREE in melts of Phase III.

Consequently, a required condition for the formation of a EGM deposit with high concentration of HREE is the saturation of alkaline magmas with respect to EGM at a stage in the magmatic evolution when the ∑LREE/∑HREE ratio was already lowered because of the fractionation of ∑LREE-rich phases, e.g., loparite-(Ce). In addition, equilibration and scavenging from a large volume of melt would favor higher concentrations of REE in EGM. If the concentration of the elements needed for saturation are significantly lower at the liquidus of the melt, then the crystallization of the ore mineral would occur at sub-liquidus conditions in small and possible partly isolated volumes of interstitial melt. Such a scenario would not facilitate the formation and accumulation of the EGM. It seems evident that the potential for viable EGM ores in the large Lovozero complex, is restricted to Phase III in which EGM crystallized as the liquidus phase in the lujavritic magma. From this follows that anhedral and interstitial EGM of the neighboring Khibiny complex EGM is unlikely to form eudialyte ore deposits, despite a bulk concentration of 531 ppm Zr [27].

5.3. Consequences for Layered Agpaitic Complexes

The evolutionary trend recorded in the EGM compositions is consistent with a continuous and closed system evolution of Lovozero intrusion and feeder system exemplified, e.g., in parageneses and clinopyroxene compositions [7]. The same is suggested for kakortokites of the Ilimaussaq intrusion based on the stratigraphic variation in EGM compositions and core to rim fractionation during in situ fractionation in crystal mushes [15].

Much information has, however, emerged over the past decade and two very different models are advocated for the development of igneous layering in Ilimaussaq, including: (1) A classic closed system evolution with layering caused by gravitational accumulation, and e.g., crystal mat formation [16,26,28–30]; and (2) a crystallization model based on repeated replenishment of the magma chamber [31]. The latter model, however, require that the magmas or mushes evolved along evolutionary trends similar to those observed in Ilimaussaq. Such models relocate observed evolution to a not known or specified feeder chamber. The need for such an unspecified feeder chambers for the Ilimaussaq intrusion rests on petrofabric (CDS) studies, sometimes sharp contacts between repeated cyclic layers, and structural characteristics interpreted as the result of turbulent accumulation of new pulses of inclusion-bearing agpaitic mush in the kakortokites [31]. It is also argued that the classic gravitational settling (or flotation) mechanisms cannot explain the petrofabrics and the repetition of 29 tripartite cycles of black, red, and white kakortokites.

These models, however, appear to exclude liquidus crystallization under the roof and subsequent gravitational accumulation of crystal mushes in the floor of the magma chamber. Magmas cool through roof and walls and are better insulated at floor by accumulated crystal mush. Cooling would in most cases be most efficient at the roof and cause crystallization and mush formation. The mushes, that would be variable affected by interaction with rafts of roof rocks, sink to the floor, and simulate being new magma pulses, although being the result of processes within the magma chamber itself. Such processes are well described from e.g., the Skaergaard intrusion [32]. At present, there is no indisputable evidence to suggest that the kakortokites of the Ilimaussaq intrusion should be anything but the result of crystallization of magma and density-controlled distribution of solids, crystal mushes, and melts within a magma chamber. The same may apply to the Lovozero complex and following Gerasimovsky et al. [1] and Kogarko et al. [17] there is no compelling evidence to suggest that the Lovozero complex represents rocks crystallized from multitude of replenishment events.

6. Conclusions

The conclusions of the study are:

1. Eudialyte (EGM) of the Lovozero complex is enriched in HREE. EGM of the ore-bearing Phase III of the complex reaches an average of 1.3 wt. % total REEs (max 1.8), and a Ce/Yb = 8.88. In addition, EGM-ores are strongly enriched with Zr and many other HFSE elements commodities.
2. The petrography shows that the time of crystallization of EGM relative to liquidus paragenesis changes upward and as the Lovozero complex crystallizes. The interstitial, anhedral EGM crystals in all of Phase II indicate that the bulk magma was not yet saturated in components needed for nucleation of EGM. Only after crystallization, about 85% of the volume of the initial magma was saturated and nucleation of EGM was reached and EGM changed the role to become a cumulus phase.
3. Saturation of the bulk magma that leads to EGM nucleation is a prerequisite for eudialyte ores. The ores formed as a result of the suspension and upward transportation of very small crystals and subsequent amalgamation growth below the roof of the magma chamber. The process compares to that suggested for the Khibina apatite-group mineral deposits [26].
4. EGM of the neighboring Khibiny complex is anhedral, interstitial, and unlikely to form eudialyte ore deposits, despite a bulk concentration of 531 ppm Zr.

Author Contributions: All scientific conceptualization, analytical work, and synthesis of the results have been carried out by the first author (L.K.), who also prepared an earlier version of the manuscript; T.F.D.N. revised the structure and wording of the manuscript, added resource perspective introduction, added petrographic definitions in description of Lovozero complex, added LREE/HREE calculation and illustration (Figure 7), added comparisons and general perspectives to the Discussion. All authors have read and agreed to the published version of the manuscript.

Funding: This work was supported by the Russian Federation represented by the Ministry of education and science of Russia № 075-15-2020-802.

Acknowledgments: We are grateful to Glasatova I.A. from GEOKHI RAS for her help in work with the database on the obtained eudialyte analyses.

Conflicts of Interest: The funders had no role in the design of the study; in the collection, analyses, or interpretation of data; in the writing of the manuscript, or in the decision to publish the results.

References

1. Gerasimovsky, V.I.; Volkov, V.P.; Kogarko, L.N.; Polyakov, A.I.; Saprykina, T.V.; Balashov, Y.A.; Brown, D.A. *The Geochemistry of the Lovozero Alkaline Massif. Part 1. Geology and Petrology*; Part 2. Geochemistry; Australian National University Press: Canberra, Australia, 1968; pp. 224–369.
2. Sørensen, H. Rhythmic igneous layering in peralkaline intrusions. An essay review on Ilímaussaq (Greenland) and Lovozero (Kola, USSR). *Lithos* **1968**, *2*, 261–283. [CrossRef]
3. Sørensen, H. Agpaitic nepheline syenites: A potential source of rare elements. *Appl. Geochem.* **1992**, *7*, 417–427. [CrossRef]
4. Sørensen, H. The agpaitic rocks—An overview. *Mineral. Mag.* **1997**, *61*, 485–498. [CrossRef]
5. Kramm, U.; Kogarko, L.N. Nd and Sr isotope signatures of the Khibina and Lovozero agpaitic centres, Kola alkaline province, Russia. *Lithos* **1994**, *32*, 225–242. [CrossRef]
6. Kogarko, L.N.; Lahaye, Y.; Brey, G.P. Plume-related mantle source of super-large rare metal deposits from the Lovozero and Khibiny massifs on the Kola Peninsula, Eastern part of Baltic Shield: Sr, Nd and Hf isotope systematics. *Miner. Pet.* **2010**, *98*, 197–208. [CrossRef]
7. Zartman, R.E.; Kogarko, L.N. Lead isotopic evidence for interaction between plume and lower crust during emplacement of peralkaline Lovozero rocks and related rare-metal deposits, East Fennoscandia, Kola Peninsula, Russia. *Contrib. Mineral. Petrol.* **2017**, *172*, 1–14. [CrossRef]
8. Marks, M.; Vennemann, T.; Siebel, W.; Markl, G. Nd-, O-, and H-isotopic evidence for complex, closed-system fluid evolution of the peralkaline Ili'maussaq intrusion, South Greenland. *Geochim. Cosmochim. Acta* **2004**, *68*, 3379–3395. [CrossRef]

9. Marks, M.A.W.; Markl, G. A global review on agpaitic rocks. *Earth-Sci. Rev.* **2017**, *173*, 229–258. [CrossRef]
10. Kogarko, L.N. Alkaline magmatism and enriched mantle reservoirs: Mechanisms, time, and depth of formation. *Geochem. Int.* **2006**, *44*, 3–10. [CrossRef]
11. Piotrowski, J.M.; Edgar, A.D. Melting relations of undersaturated alkaline rocks from South Greenland. *Medd. Grønland* **1970**, *181*, 62.
12. Kogarko, L.N.; Burnham, C.; Shettle, D. Water regime in alkaline magmas. *Geochem. Int.* **1977**, *14*, 1–8.
13. Kogarko, L.N. Ore-forming potential of alkaline magmas. *Lithos* **1990**, *26*, 165–175. [CrossRef]
14. Vlasov, K.A.; Kuzmenko, M.Z.; Eskova, E.M. *The Lovozero Alkaline Massif*; Izdatel'stvo Akademii Nauk: Moscow, Russia, 1959; 624p. (In Russian)
15. Borst, A.; Friis, H.; Nielsen, T.; Waight, T. Bulk and Mush Melt Evolution in Agpaitic Intrusions: Insights from compositional zoning in Eudialyte, Ilímaussaq Complex, South Greenland. *J. Petrol.* **2018**, *59*, 589–612. [CrossRef]
16. Cawthorn, R.G. Layering Intrusions. In *Developments in Petrology*; Elsevier Science: Amsterdam, The Netherlands; Lausanne, Switzerland; New York, NY, USA; Oxford, UK; Tokyo, Japan, 1996; Volume 15, 530p, ISBN 9780080535401.
17. Kogarko, L.N.; Williams, C.T.; Woolley, A.R. Chemical evolution and petrogenetic implications of loparite in the layered, agpaitic Lovozero Complex, Kola Peninsula, Russia. *Mineral. Petrol.* **2002**, *74*, 1–24. [CrossRef]
18. Downes, H.; Balaganskaya, E.; Beard, A.; Liferovich, R.; Demaiffe, D. Petrogenetic processes in the ultramafic, alkaline and carbonatitic magmatism in the Kola Alkaline Province: A review. *Lithos* **2005**, *85*, 48–75. [CrossRef]
19. Arzamastsev, A.A. *Unique Palaeozoic Intrusions of the Kola Peninsula. Kola Science Centre Press House*; Kola Peninsula Science Centre Press House: Apatity, Russia, 1994; 78p. (In Russian and English)
20. Kogarko, L.N.; Kononova, V.A.; Orlova, M.P.; Woolley, A.R. *Alkaline Rocks and Carbonatites of the World, Part 2*; Chapman and Hall: London, UK, 1995; 226p, ISBN 0412614403.
21. International Mineralogical Association. The Official IMA-CNMNC List of Mineral Names. The New IMA List of Minerals—A Work in Progress—Updated: November 2020. Available online: http://cnmnc.main.jp/IMA_Master_List_%282020-11%29.pdf (accessed on 16 November 2020).
22. Bussen, I.V.; Sakharov, A.S. *Petrology of the Lovozero Alkaline Massif*; Nauka: Saint Petersburg, Russia, 1972; 296p. (In Russian)
23. Johnsen, O.; Ferraris, G.; Gault, J.; Kampf, A.; Pekov, I. The nomenclature of eudialyte-group minerals. *Can. Mineral.* **2003**, *41*, 785–794. [CrossRef]
24. Chukanov, N.V.; Aksenov, S.M.; Pekov, I.V.; Belakovskiy, D.I.; Vozchikova, S.A.; Britvin, S.N. Sergevanite, $Na_{15}(Ca_3Mn_3)(Na_2Fe)Zr_3Si_{26}O_{72}(OH)_3{\cdot}H_2O$, a new eudialyte-group mineral from the Lovozero alkaline massif, Kola Peninsula. *Can. Mineral.* **2020**, *58*, 421–436. [CrossRef]
25. Schilling, J.; Wu, F.-Y.; McCammon, C.; Wenzel, T.; Marks, M.A.W.; Pfaff, K.; Jacob, D.E.; Markl, G. The compositional variability of eudialyte-group minerals. *Mineral. Mag.* **2011**, *75*, 87–115. [CrossRef]
26. Kogarko, L.N. Chemical Composition and Petrogenetic Implications of Apatite in the Khibiny Apatite-Nepheline Deposits (Kola Peninsula). *Minerals* **2018**, *8*, 532. [CrossRef]
27. Arzamastsev, A.A.; Bea, F.; Glaznev, V.N.; Arzamastseva, L.V.; Montero, P. Kola alkaline province in the Paleozoic: Evaluation of primary mantle magma composition and magma generation conditions. *Russ. J. Earth Sci.* **2001**, *3*, 1–32. [CrossRef]
28. Lindhuber, M.J.; Marks, M.A.W.; Bons, P.D.; Wenzel, T.; Markl, G. Crystal mat-formation as an igneous-layering forming process: Textural and geochemical evidence from the "lower layered" nepheline syenite sequence of the Ilímaussaq complex, South Greenland. *Lithos* **2015**, *224*, 295–309. [CrossRef]
29. Marks, M.A.W.; Markl, G. The Ilimaussaq Alkaline Complex, South Greenland. In *Layered Intrusions*; Charlier, B., Namur, O., Latypov, R., Tegner, C., Eds.; Springer: Dordrecht, The Netherlands; Heidelberg, Germany; New York, NY, USA; London, UK, 2015; pp. 649–691. [CrossRef]
30. Lauder, W. Mat formation and crystal settling in magma. *Nature* **1964**, *202*, 1100–1101. [CrossRef]

31. Hunt, E.J.; Finch, A.A.; Donaldson, C.H. Layering in peralkaline magmas, Ilfmaussaq Complex, S Greenland. *Lithos* **2017**, *268*, 1–15. [CrossRef]
32. Irvine, T.N.; Andersen, J.C.Ø.; Brooks, C.K. Included blocks (and blocks within blocks) in the Skaergaard Intrusion: Geological relations and the origins of rhythmic modally graded layers. *Geol. Soc. Am. Bull.* **1998**, *110*, 1398–1447. [CrossRef]